Available online at www.sciencedirect.com
SCIENCE DIRECT®
Cement & Concrete Composites 27 (2005) 77–84
Cement & Concrete Composites
www.elsevier.com/locate/cemconcomp

# Thaumasite formation in limestone filler cements exposed to sodium sulphate solution at 20 °C

E.F. Irassar *, V.L. Bonavetti, M.A. Trezza, M.A. González

*Civil Engineering Department, National University of Buenos Aires Centre, State, B7400JWI Olavarría, Argentina*

Received 15 October 2002; accepted 24 October 2003

**Abstract**

This paper presents a microstructural analysis of mortars made with OPC ($C_3A = 6\%$) and two SRPCs ($C_3A < 2\%$ and $C_3S = 40\%$ and 74%) containing 20% of limestone filler. Specimens analysed were immersed in $Na_2SO_4$ solution (5% w/w or 0.352 M) with pH control during two years at $20 \pm 2$ °C. The evolution of attack was determined using XRD semi-quantitative analysis on the material obtained by wearing in layers by millimetre to millimetre of the specimens. Complementary SEM and EDS studies were carried out to confirm the presence of thaumasite. Results show that OPC and high-$C_3S$ SRPC containing 20% limestone filler were found to be more susceptible to sulphate attack than the corresponding plain cement. The attack was characterised by the inward front leading first to the formation of ettringite, later formation of gypsum and finally thaumasite formation, when the decalcification of the mortar lead to the breakdown of C–S–H, providing the required silica. The reaction sequence in Portland limestone cements is essentially the same as in plain Portland cements. The main change is that thaumasite is formed at later stages with decomposition of the ettringite formed during the firsts stage of attack. In SRPC with low $C_3S$, the attack was limited to the first millimetres and the thaumasite was not detected.


*Keywords:* Sulphate attack; Limestone filler; Microstructural analysis; SRPC; Thaumasite

## 1. Introduction

The formation of thaumasite is recognised as a cause of deterioration of Portland cement based products. It has been identified as a deterioration compound in historical buildings [1] and as the last stage of deterioration in marine structures [2]. According to the literature [3], there are two mechanisms of thaumasite formation in mortar and concrete. First, it can be derived from the evolution of ettringite when it incorporates $Si^{4+}$ into its structure, substituting the $Al^{3+}$ ions, and the interstitial replacement of $[(SO_4^{2-})_3\ (H_2O)_2]$ by $[(SO_4^{2-})_2\ (CO_3^{2-})_2]$. Secondly, the thaumasite is the result of the interaction between sulphate and carbonate ions and the C–S–H gel.

Since 1980, the increase of limestone filler addition during the manufacture of cement has contributed to increase the interest studying thaumasite formation in concretes exposed to sulphate environments. In this case, the limestone filler is the internal source that provides the carbonate ions needed for thaumasite formation. The rate of this reaction is greatly increased at cold temperature below 15 °C.

The concrete at risk from this type of sulphate attack includes those made with sulphate resistant Portland cement. Several concretes designed to provide good sulphate resistance have been affected by thaumasite formation according to Crammond and Halliwell [4].

The bibliographic review about sulphate performance of Portland limestone cement (PLC) shows different trends according to the $C_3A$ content in cement, the percentage of limestone filler added and the condition of sulphate environment (temperature, pH control, and concentration and type of sulphate). Some authors [5,6] conclude that the incorporation of filler increases the sulphate resistance of cement, while others [7–10] conclude that limestone filler addition produces a decrease in sulphate resistance of cements.

South-American regions have a mild climate, the mean temperature is in the range of 15–30 °C, and the

* Corresponding author. Tel.: +54-228-445-1055; fax: +54-228-445-0628.
*E-mail address:* firassar@fio.unicen.edu.ar (E.F. Irassar).

0958-9465/$ - see front matter © 2004 Elsevier Ltd. All rights reserved.
doi:10.1016/j.cemconcomp.2003.10.003

production of PLC containing up to 20% of limestone filler has growth during the last years. For this reason, it is important to determine the formation of thaumasite in PLC exposed to sulphate solution at temperature above 15 °C. In concrete foundations, the risk of thaumasite formation is increased because it is likely to occur the presence of sulphate ground waters at cold temperature below 15 °C.

This paper reports the results of microstructural analysis of mortar made with different Portland cements stored in sodium sulphate solution for up to two years. A comprehensive analysis of the sequence of attack and the causes of thaumasite formation are presented.

## 2. Materials and procedures

### 2.1. Mortar specimens examined

The specimens analysed were made with ordinary Portland cement (OPC) and two sulphate resistant Portland cements with very different $C_3S$-content ($SRPC_{low}$ and $SRPC_{high}$). The physical and chemical characteristics of the cements are detailed in Table 1. For all cements, the ASTM C 452 expansion at 14 days was lower than the limit for sulphate resistant Portland cement (0.04%). Portland limestone cements were produced by mixing limestone filler (20% by weight) with each Portland cement. Limestone filler (LF) contains 85% of $CaCO_3$ in calcite form without clay minerals. The main impurity was quartz ($SiO_2 = 11\%$) and it was ground at a Blaine fineness of 710 $m^2/kg$.

Table 1
Chemical composition and physical properties of Portland cements used

| | $SRPC_{low}$ | $SRPC_{high}$ | OPC |
|---|---|---|---|
| *Chemical composition, % in weight* | | | |
| $SiO_2$ | 23.66 | 21.00 | 22.19 |
| $Al_2O_3$ | 3.00 | 3.29 | 4.08 |
| $Fe_2O_3$ | 5.41 | 4.68 | 3.16 |
| CaO | 62.14 | 66.00 | 62.74 |
| MgO | 0.60 | 0.67 | 0.58 |
| $SO_3$ | 1.59 | 2.20 | 2.48 |
| Alkalis | 0.72 | 0.82 | – |
| Loss by ignition | 1.61 | 1.23 | 1.86 |
| *Composition (Bogue), % in weight* | | | |
| $C_3S$ | 40 | 74 | 51 |
| $C_2S$ | 38 | 4 | 26 |
| $C_3A$ | 0 | 1 | 6 |
| $C_4AF$ | 15 | 14 | 10 |
| Fineness blaine, $m^2/kg$ | 313 | 306 | 285 |
| *Compressive strength, MPa* | | | |
| 3 days | 11.4 | 27.3 | 23.3 |
| 7 days | 17.6 | 29.2 | 35.8 |
| 28 days | 32.7 | 32.5 | 42.8 |
| *Expansion (ASTM C 452), %* | | | |
| 14 days | 0.015 | 0.012 | 0.023 |
| 90 days | 0.025 | 0.021 | 0.048 |
| 360 days | 0.030 | 0.045 | 0.162 |

Mortar bars ($285 \times 25 \times 25$ mm) were cast according to ASTM C 1012 (sand to cementitious material ratio of 2.75 and water to cementitious ratio of 0.485). Specimens were stored in a moist cabinet during 24 h, then they were removed from the mould and cured in saturated lime-water until to achieve $30 \pm 3$ MPa compressive strength. At this age, mortar bars of Portland and PLC cements were stored in individual plastic tanks (mortar bars volume to sulphate–solution volume 1:4) containing $Na_2SO_4$ (5% w/w or 0.352 M) at pH-constant ($7 \pm 1$) for a period of 2 years at laboratory temperature ($20 \pm 2$ °C). The pH of test solution was periodically readjusted by titration with a combined solution (0.35 M $Na_2SO_4$ + 2 N $H_2SO_4$) using a few drops of phenolphthalein as pH-indicator. The volume of titration of solution added was registered. Complete details on sulphate performance, strength development and sulphate demand of PLCs were reported previously [7,8].

### 2.2. Layer by layer analysis

The compound profile was determined in mortar specimens after 2 years of sulphate immersion. The technique used was as follow: The specimens were tested and the remaining slices were dried at 40 °C over a period of 7 days. Subsequently, using a wearing device, layers of 1-mm depth were obtained from the cast surface to the core of the specimens The powdered material was obtained by cutting perpendicularly to the prism face at 5 mm from both edges of the prism (Fig. 1). The depth of each layer was selected at 1 mm because the sand used in making the mortar passed through a 1.18 mm (No. 16) sieve. For this layer depth, the sample is representative of the compound formed in all structure of mortar including both paste and interfaces. After layer grinding, the material was collected and sieved through a 75 μm (No. 200) sieve to removed the bulk of sand grains. Finally, the material was ground to pass the 45 μm (No. 325) sieve and stored in a desiccator to minimise carbonation before XRD analysis.

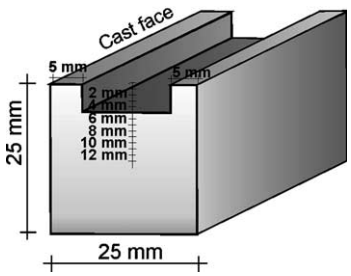


Fig. 1. Diagram of the profile sampling in mortar bars.

### 2.3. XRD analysis

XRD measurements were performed on a Philips X'Pert diffractometer equipped with a graphite monochromator using CuKα radiation and operating at 40 kV and 20 mA. Step scanning was used with a scan speed of 2°/min and sampling interval of 0.02° 2θ. The powder sample was loaded into the diffractometer sample holders from the back to avoid the preferred orientation effect on ettringite and CH crystals [11]. To determine the amount of ettringite, gypsum, CH and $CaCO_3$ present in each mortar layer, the semi-quantitative XRD analysis was made using the internal standard model supplied by the APD software package. The peak used to quantify these phases were: ettringite at 9.08° 2θ, gypsum at 11.59° 2θ, CH at 18.04° 2θ and $CaCO_3$ at 29.4° 2θ.

## 3. Results

### 3.1. Expansion

In this paper, the evolution of expansion is presented as illustration of sulphate attack on mortar, but the complete details can be found elsewhere [7,8]. Fig. 2 summarised the expansion of mortars with 0% and 20% of LF in sulphate solution up to 2 years for the three cements used. These data indicate that $SRPC_{low}$ mortar has the lowest expansion, while $SRPC_{high}$ mortar has a high expansion, similar to OPC mortar, despite of the low $C_3A$-content in this cement. For all cement, mortars containing 20% of LF have a larger expansion compared to the corresponding plain mortar.

### 3.2. Compound profiles

After 2 years of immersion in sodium sulphate solution at 20 ± 2 °C, profiles of attack products quantified by XRD are illustrated in Figs. 3–6 for OPC, OPC + 20%LF, $SRPC_{low}$ + 20%LF and $SRPC_{high}$ + 20%LF mortars, respectively. In all profiles, the *sulphate attack transition zone* described by Wang [12] can be observed. In this zone, the composition and amount of hydration products have dramatically changed. Ettringite has bell shape distribution from the surface to the core of specimens and there is a reverse relationship between the distribution of gypsum and CH intensity peaks. The gypsum peaks have a maximum near the surface and they decrease rapidly to zero inside the specimens, while the intensity of the CH peak increases from zero at the surface to a maximum in the centre of specimens. The distribution of calcium carbonate decreases from a maximum at the surface to the level of carbonate addition at the core of specimen.

For the mortar made with OPC (Fig. 3), the profile illustrates that the depth of the *sulphate attack transition zone* was approximately 4–5 mm after 2 years. Ettringite was detected at 12-mm depth and the shape of the main ettringite peak (9.08° 2θ) and the absence of some characteristic peaks (16.0° and 19.36° 2θ) suggests no thaumasite formation due to the carbonation of this mortar as revealed by XRD analysis. The detailed XRD-pattern showed the absence of other characteristic peaks of thaumasite. The presence of gypsum accompanied by the depletion of CH has a depth of 4 mm. In this mortar, $CaCO_3$ could have formed due to carbonation when specimens were removed from solution.

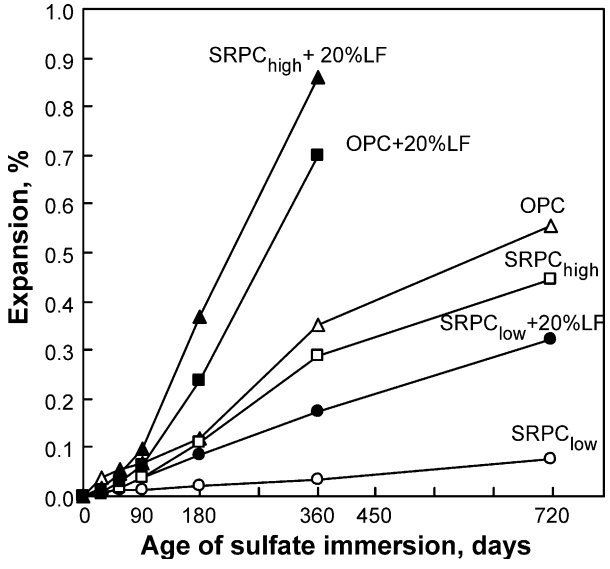


Fig. 2. Expansion of mortar immersed in sodium sulphate solution.

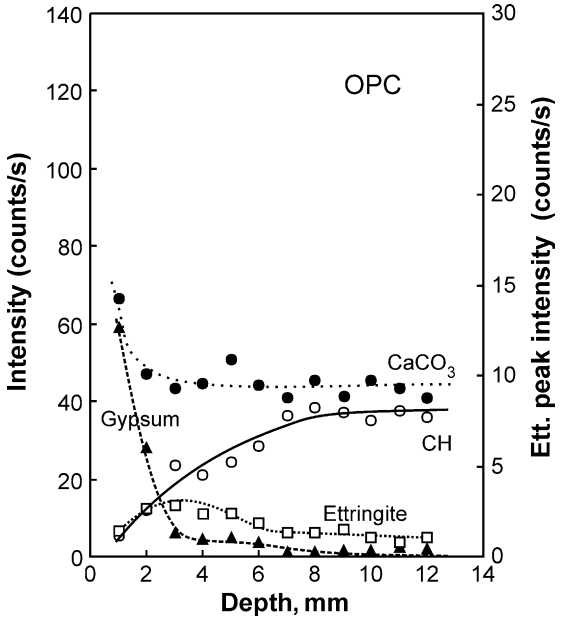


Fig. 3. Compound profile in OPC mortar.

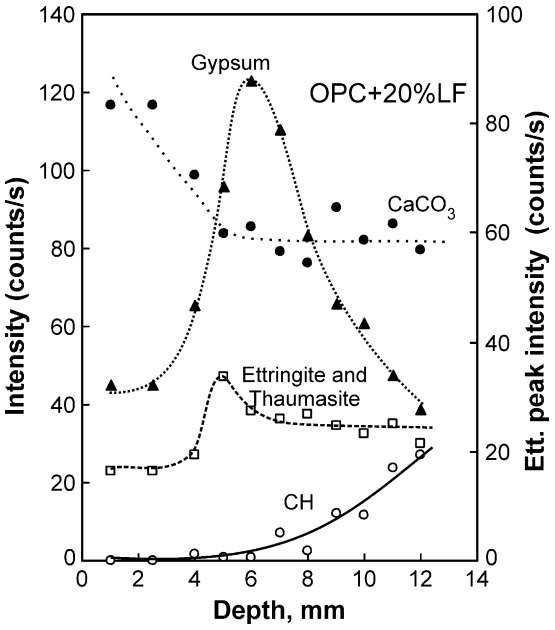


Fig. 4. Compound profile in OPC + 20%LF mortar.

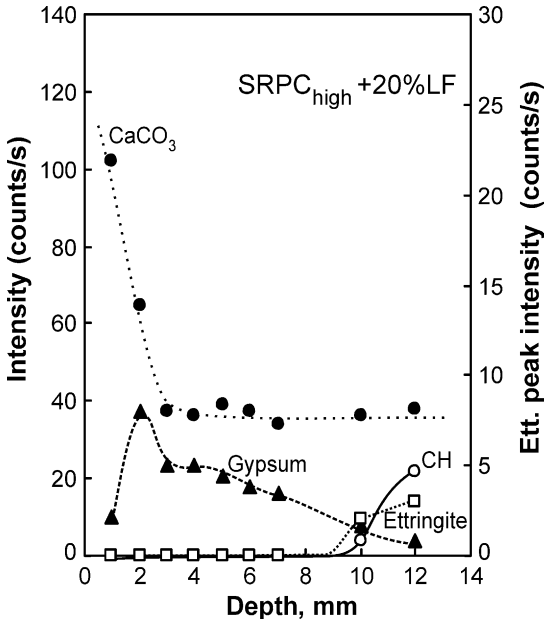


Fig. 6. Compound profile in $SRPC_{high}$ + 20%LF mortar.

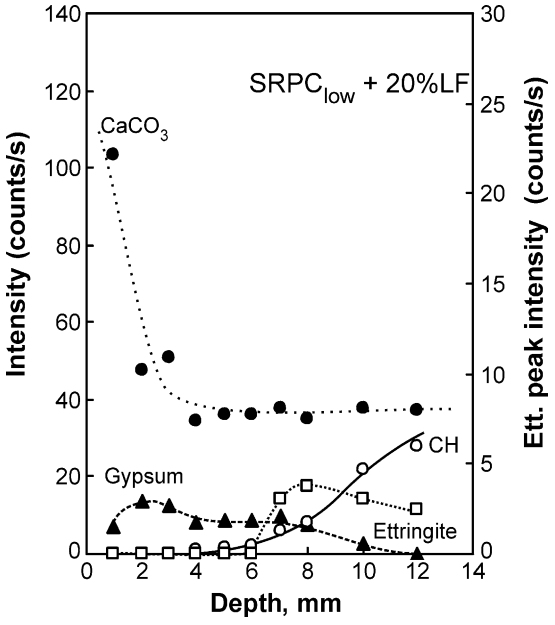


Fig. 5. Compound profile in $SRPC_{low}$ + 20%LF mortar.

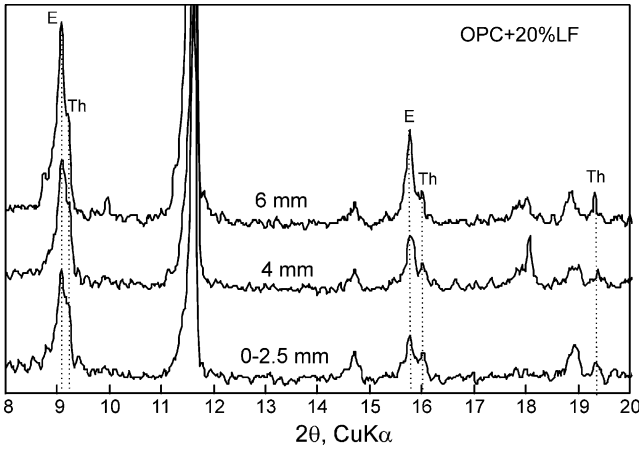


Fig. 7. Details of XRD pattern in OPC + 20%LF mortar showing the characteristic peaks of thaumasite (E = ettringite, Th = thaumasite).

The profile of OPC + 20%LF mortar (Fig. 4) shows that the complete section of specimens was altered by sulphate attack after 2 years. A very strong peak of ettringite–thaumasite (9.08–9.24° 2$\theta$) was identified in all layers analysed. The amount of ettringite–thaumasite quantified was four times higher in this sample than in the sample of OPC mortar. The presence of thaumasite was detected in the XRD pattern (see Fig. 7) by the deformation of the main peaks (9.24° and 16.0° 2$\theta$) and its characteristic peak at 19.35° 2$\theta$ on the superficial layer (1–2 mm). From 4- to 6-mm layers, the deformation of the ettringite peak attributable to thaumasite formation was also detected. The lack of CH was determined from the surface to 6-mm depth and it presents a large proportion of gypsum. Also, gypsum is present throughout the specimen and it has a bell shape distribution with a maximum at 6-mm depth.

For $SRPC_{low}$ + 20LF mortar (Fig. 5), the compound profile shows the formation of gypsum as the principal product of sulphate attack from the surface of specimen to 8–10 mm layers. However, the amount of gypsum determined is less than that determined for OPC + 20%LF mortar. CH was detected from 4 to 5 mm depth to the core of specimens. It also exhibits slight ettringite peaks from 6 to 12 mm, while there is no evidence of the presence of thaumasite peaks in the

XRD patterns. The carbonation was restricted to the first millimetres for the surface of specimens.

$SRPC_{high}$ + 20%LF profile (Fig. 6) presents a maximum in gypsum distribution and its amount is four times greater than the corresponding amount obtained for the $SRPC_{low}$ + 20%LF profile. It was detected throughout the section of mortar and the complete depletion of CH was detected from the surface to a depth of 10 mm. Carbonation is also presented from 1- to 3-mm layers. Neither ettringite nor thaumasite was detected in this mortar. However, ettringite was detected on bulk samples of mortars in previous analyses at 1-year [7].

## 4. Discussion

Microstructural analyses presented indicate that sulphate attack in ASTM C 1012 mortars is a degradation process progressing from the surface to the core of specimen. These data agree closely with the mechanism of sulphate attack proposed by Gollop and Taylor [13] and the early stages of attack reported by Wang [12]. The sequence of attack has the following stages: (1) Diffusion of sulphate ions and CH leaching, (2) ettringite formation, (3) gypsum formation and depletion of CH, (4) decalcification of C–S–H and (5) thaumasite formation. This attack sequence is similar to that reported by Hartshorn et al. [9] in spite of the different type and temperature of the solution.

(1) After immersion in solution, two counter ion flows are established: the $(OH)^-$ diffuse from the inside mortar to solution and the $SO_4^{2-}$ diffuse from the solution to the interior of the mortar [14]. This causes the declining rate of titration solution added to maintain the pH of storage solution. As reported in a previous paper [7], all mortars with 20% of LF increase the rate and the total volume added of titration solution showing an extended interaction of the mortar-sulphate solution system.

(2) Ettringite is formed by the reaction of sulphate ions with the AFm phase (monosulfoaluminate and monocarboaluminate) present in the OPC and OPC + 20%LF mortar previously to sulphate immersion as reveal the XRD patterns showed in Fig. 8. For SRPC cements, ettringite can also be formed by reaction between sulphate ions and ferroaluminate phase [15]. XRD profiles corroborate that ettringite is the first attack product detected in the vanguard of attack front. It shows that all mortars have the same sequence of attack. Ettringite was found deposited in zones around the aggregates (Fig. 9), filling the transition space or the space created by the cracking due to the localised expansion. This situation is attributable to the secondary mineralization described by Bonen [16]. Ettringite is decomposed beyond the surface, because it is an

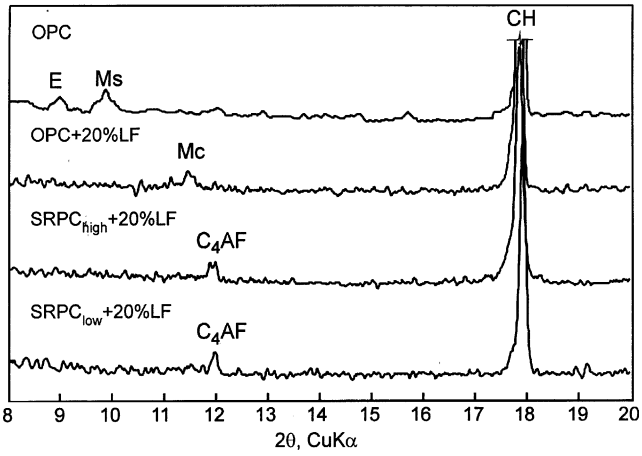


Fig. 8. XRD pattern of mortar before the sulfate immersion (Ms = calcium monosulfoaluminate, Mc = calcium monocarboaluminate, $C_4AF$ = tetracalcium alumino ferrite).

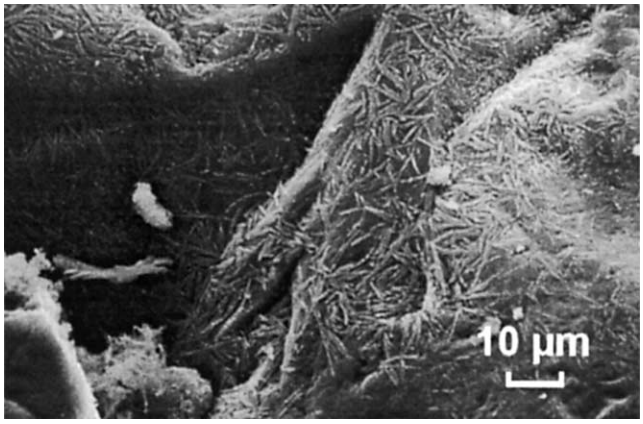


Fig. 9. SEM photograph of ettringite at paste–aggregate interface in OPC + 20%LF mortar after 2 years.

unstable compound when the pH falls below 10.7 [17]. The pH reduction in the pore solution may be caused by the pH control in the solution or by carbonation of the mortar. An increase of $CaCO_3$ content at the surface of specimens could be attributed to some carbonation occurred during immersion solution, possibly because of the presence of $CO_2$ dissolve in sulphate solution.

(3) Gypsum crystallisation begins when the alumina supplied by the AFm phase to the pore solution is deficient and the ettringite crystallisation ceases [18]. Consequently, the sulphate ions react with $Ca^{2+}$ ions and more CH is decomposed in the pores causing the CH depletion. In all profiles, gypsum was generally detected at preceding layers with the layer corresponding to the maximum of ettringite distribution. This sequence of reactions is typical in mortars containing AFm phase prior to sulphate immersion (see Fig. 8). The formation of gypsum causes the softening of the external layer of mortar while the interior of the matrix remains cohesive. For SRPC cements, the sulphate attack is a

phenomenon involving several stages (induction, gypsum formation and ettringite formation) as reported in previous paper using these cements [15]. According to the dominating mechanism detected by XRD techniques, instead of the processes beginning simultaneously, the ettringite crystallisation cannot be detected before the gypsum formation, and gypsum prevails as the first product of chemical reaction. However, Gollop and Taylor [14] suggest that the sequence should be identical to that in OPC cement, but the reaction to form ettringite occurs only within the cement paste, and its crystals can have a submicrometer dimension not detectable by XRD.

Precipitation of CH causes massive deposits of crystals on the paste–aggregate interface, which leads to inevitable increase of porosity in this region. Bensted [19] emphasises that the limestone filler grains modify the paste microstructure and the topochemical growth of CH upon $CaCO_3$ crystal might occur and hence facilitate the access of $SO_4^{2-}$ ions to form gypsum. Also, limestone filler increases the hydration rate of Portland cement leading to the precipitation of CH located around the filler grains and the aggregate surfaces, but it does not contribute to the later CH reduction in the transition zone as active mineral admixture such as granulated blast furnace slag.

Finally, when the outer layer of mortar presents a dominant gypsum environment due to the continuous removal of CH, the $OH^-$ concentration into the pores would decay producing the instability of C–S–H. According to Mehta [18], when the C–S–H is surrounded with crystalline gypsum instead of crystalline CH, it starts to loss strength and stiffness causing a loss in cohesion of cement matrix. Under this condition the ettringite crystals become more expansive increasing the cracking and the permeability. When all CH was removed, the amount of gypsum may decrease in the corroded surface due to the decomposition of the solid phase containing sulphate and the carbonation increases.

(4) In the outer transition zone, mortars contain little or no CH and this compound is needed to preserve the integrity of C–S–H by creating a surrounding environment with high pH. In OPC + 20%LF profile, it can be observed that CH was fully depleted and the gypsum environment was detected at several millimetres below the surface. Consequently, C–S–H may be affected causing progressive decalcification that produces changes in the chemical and microstructural composition [13,16]. When pastes or mortars are stored in strong $MgSO_4$ solution, the deleterious effect of attack is due to the combined aggression of $Mg^{2+}$ and $SO_4^{2-}$ accompanied by the formation of magnesium hydroxide, gypsum and C–S–H decomposition. The reaction of $Mg^{2+}$ and $SO_4^{2-}$ with the CH causes the formation and precipitation of magnesium hydroxide and gypsum until the CH depletion is completed. Following the consumption of CH, the $Ca^{2+}$ is provided by the decalcification of C-S-H causing its breakdown and increasing the rate of deterioration [9,16].

(5) According to Collepardi [1], the formation of thaumasite is due to the reaction of calcium carbonate, calcium sulphate, C–S–H and water. In $Na_2SO_4$ solution, decomposition of C–S–H appears to be the source of the former silica available in the pore solution that reacts with the calcium carbonate from the limestone filler and the sulphate ions from aggressive solution to form the thaumasite.

Fig. 10 illustrates the alteration of microstructure near the surface (spalled zone) of OPC + 20%LF mortar after two years. Composition determined by EDS is very close to the thaumasite compound. At 3–4 mm depth, massive crystals containing silica and alumina were found. It indicates that thaumasite–ettringite crystals coexist as a limited solid solution or ettringite exerts a catalytic effect on thaumasite formation [3]. This situation will usually be the case for Portland cement with high or moderate $C_3A$ content as used in this experience. These cements can produce a lot of ettringite whose formation always precedes that of thaumasite.

For $SRPC_{low}$, ettringite was detected at 6-mm depth, but it cannot be found up to 10-mm layer in $SRPC_{high}$ after two years. The lack of ettringite at the first millimetres in the altered zone could be the cause for the

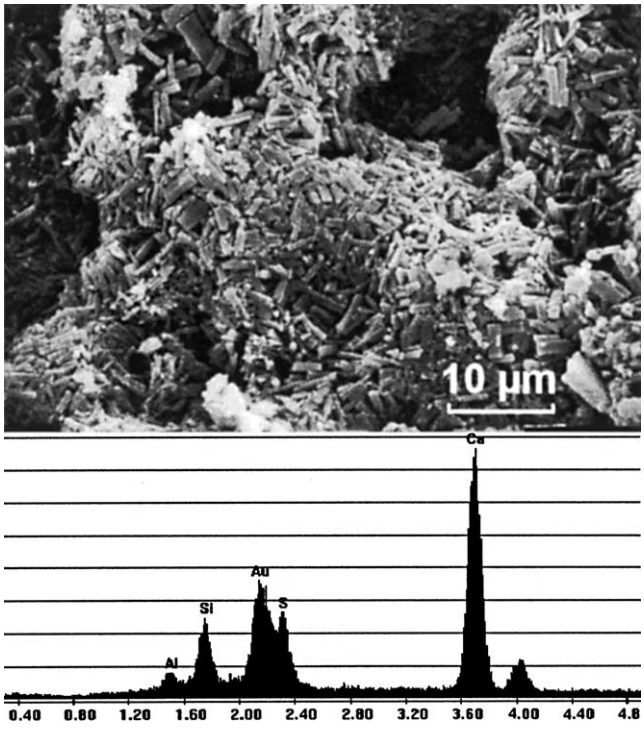


Fig. 10. SEM photograph of thaumasite formation near the surface in OPC + 20%LF mortar after 2 years. EDS spectrum shows that the height peaks for Si, S, Ca and Al are those that would be expected for thaumasite.

absence of thaumasite. According to the authors' opinion, thaumasite is not present because its formation at 20 °C follows the first formation of ettringite caused by sulphate attack. In these plain mortars, ettringite was detected containing some proportion of Fe in its composition after 1 year [15].

In the deeper attack front, compound profiles show that ettringite formation is the first compound detected by the XRD analysis; while the final stage of attack occurs in the outer surface and it is characterised by the presence of thaumasite. However, this situation was different for SRPC cements.

Bensted [20] states that thaumasite forms below 15 °C, especially at about 10 °C or less, ideally within the range 0–5 °C under cold damp conditions. Also, he suggested that this reaction does not occur to any perceptible extent at about 20 °C or above. However, Diamond [21] reports that significant contents of thaumasite have been found in a building located in Southern California, a region with mild temperatures. Ludwing and Mehr [22] found that the formation of ettringite is decisive at 20 °C and only after longer storage time (600 days) did thaumasite occur. XRD, SEM and EDS analyses presented here on samples near the surface of OPC + 20%LF mortars confirm the presence of thaumasite at (20 ± 2 °C) as the final stage of sulphate attack.

Preliminary results of cement pastes containing SRPC ($C_3A = 2\%$, $C_3S = 58\%$) and SRPC + 18%LF stored in a combined solution (0.176 M $MgSO_4$ and 0.176 M $Na_2SO_4$; pH = 7 ± 1)) at 5 and 20 °C, showed that the degradation process is more extensive at low temperature in accordance with results obtained by Harstshorn et al. [23]. But, the XRD-layer analysis (Fig. 11) does not reveal the formation of thaumasite after one year of immersion. Ettringite is easily detected on all analysed layers (1–4 mm) of SRPC and SRPC + 18%LF at both temperature of solution. For SRPC + 18%LF, it can be observed the gradual consumption of calcium monocarboaluminate form surface to 4-mm layers. However, XRD patterns reveal the presence of strong peak of CH at $2\theta = 18.01°$ for both cements stored at 5 and 20 °C, suggesting that the thaumasite formation requires previous C–S–H breakdown caused by the complete CH depletion in the paste.

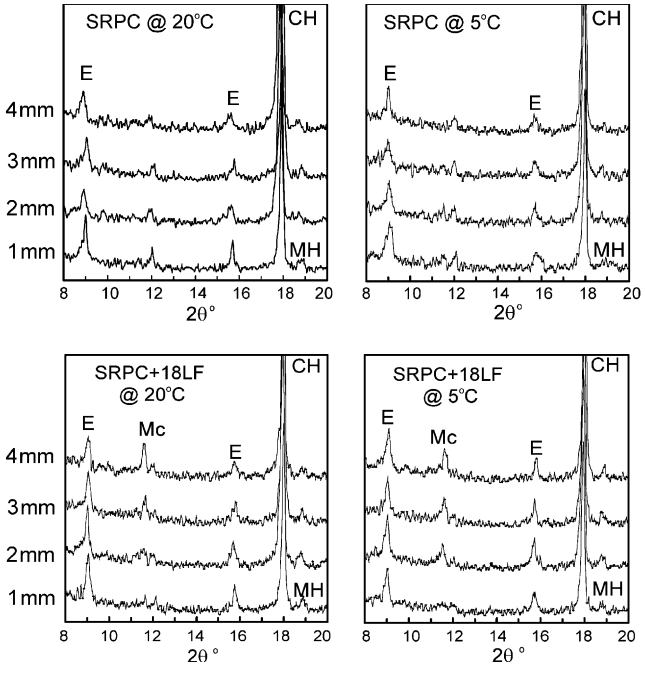


Fig. 11. XRD patterns of layers obtained from cement pastes stored in combined sulphate solution at 20 and 5 °C (E = ettringite, CH = calcium hydroxide, MH = magnesium hydroxide, Mc = calcium monocarboaluminate).

## 5. Conclusion

1. The attack in mortars containing limestone filler is characterised by an inward movement of the reaction front leading first to the formation of ettringite, later to gypsum deposition and finally to thaumasite formation when the decalcification of the mortar leads to the breakdown of C–S–H providing the required silica.
2. The reaction sequence in limestone filler cement is essentially the same as in the case of Portland cement. The main change is that at later stages, thaumasite is formed with decomposition of the first formed ettringite at 20 ± 2 °C. It revels that the formation of thaumasite does not limited to low temperature.
3. Thaumasite cannot be detected in both SRPCs (zero—$C_3A$) containing limestone filler, suggesting that the previous formation of ettringite could be necessary to the later formation of thaumasite at 20 °C.

## Acknowledgements

Results presented in this paper correspond to the research project PICT97 12-00000-01323 supported by the Agencia Nacional de Promoción Científica y Técnica and the Secretaría de Ciencia y Técnica de la Universidad Nacional del Centro de la Provincia de Buenos Aires.

## References

[1] Collepardi M. Thaumasite formation and deterioration in historic buildings. Cem Concr Comp 1999;21(2):147–54.
[2] Regourd M, Bissery P, Evers G, Hornain H, Mortureux B. Ettringite et thaumasite dans le mortier de la digue du port de Cherbourg. Annal ITBTP 1978;358:1–14.

[3] Grijalvo JA, Blanco-Varela MT, Maroto FP, Sanchez AP, Moreno TV. Thaumasite formation in hydraulic mortars and concretes. In: Malhotra VM, editor. Proceeding Fifth International Conference Durability of Concrete, Barcelona. Spain, ACI SP 192, 2000. p. 1173–89.
[4] Crammond NJ, Halliwell, MA. The thaumasite form of sulfate attack in concretes containing a source of carbonate ions—a microstructural overview. In: Second CANMET/ACI International Symposium on Advances in Concrete Technology, Las Vegas, USA. ACI SP 154, 1995. p. 357–80.
[5] Piasta G, Sawicz Z, Koprowski G, Owsiak Z. Influence of limestone powder filler on microstructure and mechanical properties of concrete under sulphate attack. In: Proceeding 10th International Congress of Chemistry of Cement, Sweden, 1998. 4iv018, p. 8.
[6] Zelic J, Krstulovic R, Tkalcec E, Krolo P. Durability of the hydrated limestone–silica fume Portland cement mortars under sulphate attack. Cem Concr Res 1999;29(6):819–26.
[7] González MA, Irassar EF. Effect of limestone filler on the sulfate resistance of low $C_3A$ Portland cement. Cem Concr Res 1998;28(11):1655–67.
[8] Irassar EF, González M, Rahhal V. Sulphate resistance of Type V cements with limestone filler and natural pozzolan. Cem Concr Comp 2000;22(5):361–8.
[9] Hartshorn SA, Sharp JH, Swamy RN. Thaumasite formation in Portland-limestone cement pastes. Cem Concr Res 1999;29(8): 1331–40.
[10] Brosoi A, Collepardi S, Copolla L, Troli R, Collepardi M. Sulfate attack on blended Portland cement, In: Malhotra VM, editor. Proceeding Fifth International Conference Durability of Concrete, Barcelona. ACI SP 192, USA, 2000. p. 417–32.
[11] Crammond NJ. Quantitative X-ray diffraction analysis of ettringite, thaumasite and gypsum in concrete and mortars. Cem Concr Res 1985;15:431–41.
[12] Wang JG. Sulfate attack on hardened cement paste. Cem Concr Res 1994;24(4):735–42.
[13] Gollop RS, Taylor HFW. Microstructural and microanalytical studies of sulfate attack. I. Ordinary Portland cement paste. Cem Concr Res 1992;22(6):1027–38.
[14] Gollop RS, Taylor HFW. Microstructural and microanalytical studies of sulfate attack: III—Sulfate resistant Portland cement: reaction with sodium and magnesium sulfate solution. Cem Concr Res 1995;25(7):1581–90.
[15] González MA, Irassar EF. Ettringite formation in low $C_3A$ Portland cement exposed to sodium sulfate solution. Cem Concr Res 1997;27(7):1061–72.
[16] Bonen D. A microstructural study of the effect produced by magnesium sulfate on plain and silica fume-bearing Portland cement mortars. Cem Concr Res 1993;23(3):541–53.
[17] Gabrisova A, Havlica J, Sahu S. Stability of calcium sulphoaluminate hydrates in water solutions with various pH values. Cem Concr Res 1991;21(6):1023–7.
[18] Mehta PK. Mechanism of sulfate attack on Portland cement concrete—another look. Cem Concr Res 1983;13(3):401–6.
[19] Bensted J. A discussion of the paper: Studies about a sulfate resistant cement: influence of Admixtures. Cem Concr Res 1995;25(5):1129–30.
[20] Bensted J. Thaumasite—background and nature in deterioration of cements, mortars and concretes. Cem Concr Comp 1999;21(2):117–21.
[21] Diamond A. Microscopic Features of ground water induced sulfate attack in highly permeably concretes. In: Malhotra VM, editor. Proceeding Fifth International Conference Durability of Concrete, Barcelona. ACI SP 192, 2000. p. 403–16.
[22] Ludwig U, Mehr S. Destruction of historical buildings by formation of ettringite and thaumasite. In: Proceeding. 8th International Congress of Chemistry Cement, Brazil, 1986. p 181–8.
[23] Hartshorn SA, Sharp JH, Swamy RN. The thaumasite form in Portland-limestone cement mortars stored in magnesium sulfate solution. Cem Concr Comp 2002;24(4):351–9.